Am J Physiol Heart Circ Physiol 310: H839–H846, 2016.
First published January 29, 2016; doi:10.1152/ajpheart.00728.2015.

CALL FOR PAPERS | *Quantitative Analyses of Coronary Vascular and Cardiac Mechanics in Health and Disease*

Influence of segmented vessel size due to limited imaging resolution on coronary hyperemic flow prediction from arterial crown volume

P. van Horssen,[1]* M. G. J. T. B. van Lier,[1]* J. P. H. M. van den Wijngaard,[1] E. VanBavel,[1] I. E. Hoefer,[2] J. A. E. Spaan,[1] and M. Siebes[1]

[1]*Department of Biomedical Engineering and Physics, Academic Medical Center, University of Amsterdam, Amsterdam, The Netherlands; and* [2]*Department of Experimental Cardiology, Utrecht Medical Center, Utrecht, The Netherlands*

Submitted 16 September 2015; accepted in final form 19 January 2016

van Horssen P, van Lier MG, van den Wijngaard JP, VanBavel E, Hoefer IE, Spaan JA, Siebes M. Influence of segmented vessel size due to limited imaging resolution on coronary hyperemic flow prediction from arterial crown volume. *Am J Physiol Heart Circ Physiol* 310: H839–H846, 2016. First published January 29, 2016; doi:10.1152/ajpheart.00728.2015.—Computational predictions of the functional stenosis severity from coronary imaging data use an allometric scaling law to derive hyperemic blood flow (Q) from coronary arterial volume (V), $Q = \alpha V^{\beta}$. Reliable estimates of α and β are essential for meaningful flow estimations. We hypothesize that the relation between Q and V depends on imaging resolution. In five canine hearts, fluorescent microspheres were injected into the left anterior descending coronary artery during maximal hyperemia. The coronary arteries of the excised heart were filled with fluorescent cast material, frozen, and processed with an imaging cryomicrotome to yield a three-dimensional representation of the coronary arterial network. The effect of limited image resolution was simulated by assessing scaling law parameters from the virtual arterial network at 11 truncation levels ranging from 50 to 1,000 μm segment radius. Mapped microsphere locations were used to derive the corresponding relative Q using a reference truncation level of 200 μm. The scaling law factor α did not change with truncation level, despite considerable intersubject variability. In contrast, the scaling law exponent β decreased from 0.79 to 0.55 with increasing truncation radius and was significantly lower for truncation radii above 500 μm vs. 50 μm ($P < 0.05$). Hyperemic Q was underestimated for vessel truncation above the reference level. In conclusion, flow-crown volume relations confirmed overall power law behavior; however, this relation depends on the terminal vessel radius that can be visualized. The scaling law exponent β should therefore be adapted to the resolution of the imaging modality.

allometric scaling laws; coronary blood flow; blood volume; imaging cryomicrotome; intramural coronary arteries

NEW & NOTEWORTHY

This study confirms an allometric scaling law behavior between stem hyperemic blood flow (Q) and arterial crown volume (V), $Q = \alpha V^{\beta}$. However, this relation depends on the terminal vessel diameter at which the tree is truncated. The exponent β should therefore be adapted to the resolution of the imaging modality.

FRACTIONAL FLOW RESERVE (FFR) has been shown to be a reliable and a widely accepted method to assess whether a coronary artery stenosis is responsible for myocardial ischemia (11). Conceptually, FFR is defined as the hyperemic flow in a vessel with a stenosis relative to the hypothetical hyperemic flow in the undiseased vessel. In practice, FFR is measured invasively as the ratio between pressure distal to a stenosis and aortic pressure, during adenosine-induced hyperemia. This requires passing of a guide wire with a pressure sensor through the stenosis. Despite the reliability of this method, risks of vessel and plaque rupture, procedure time, and costs have inspired the search for new less-invasive alternatives for assessing FFR (18), based on computational methods applied to arterial models obtained from angiography (27) or CT (6). By using experimentally established form-function relationships, coronary flow can be calculated from image-derived morphological data. These relationships are expressed in terms of allometric scaling laws relating, among others, coronary flow to myocardial mass (1), cumulative arterial branch length, stem diameter, or the total crown volume, as summarized elsewhere (4). Using this last method, FFR prediction is based on the hypothetical flow in the absence of the stenosis, as estimated from the luminal volume of the arterial tree distal to the stenosis (7). The rationale of this approach is that larger vascular trees perfuse larger myocardial volumes and therefore transport more flow. Using allometric scaling laws, Molloi and Wong (8) established that hyperemic flow (Q) at any point in the coronary arterial tree is related to the total volume of the distal arterial tree (V) as $Q = \alpha V^{\beta}$, with allometric exponent β and scaling factor α (8). Meaningful application of this relation for FFR prediction requires reliable values for α and β. Several studies have been performed to provide such estimates, based on comparison with measured flow (31), or using scaling laws applied to coronary vascular trees extracted from microcomputed tomography images (6). However, the proposed values deviate to an extent that hampers their use in deriving hyperemic flow from image-based arterial tree volumes. A particular concern here is the effect of limited

* P. van Horssen and M. G. J. T. B. van Lier contributed equally to this work.

Address for reprint requests and other correspondence: M. Siebes, Dept. of Biomedical Engineering and Physics (BMEP), Academic Medical Center, Univ. of Amsterdam, Meibergdreef 9, 1105 AZ Amsterdam, The Netherlands (e-mail: m.siebes@amc.uva.nl).

0363-6135/16 Copyright © 2016 the American Physiological Society

Downloaded from http://ajpheart.physiology.org/ by 10.220.33.2 on January 3, 2017

imaging resolution associated with clinical imaging modalities.

We hypothesized that FFR prediction based on allometric scaling laws applied to image-based anatomic vessel reconstructions requires a resolution-dependent allometric flow-volume relation. The relation between hyperemic flow in healthy canine coronary vessels and the volume of the distal arterial tree was therefore determined for a range of simulated imaging resolutions. Flow distribution was assessed by microsphere injections, and arterial lumen volume was determined from high-resolution 3D reconstructions of the coronary vascular bed. The impact of the resulting allometric scaling law relations on hyperemic flow and FFR was assessed.

Glossary

3D	Three-dimensional
α	Scaling factor
β	Allometric exponent
FFR	Factional flow reserve
FFRct	Fractional flow reserve derived from computed tomography
FFR_{ref}	Reference fractional flow reserve
i	Individual segment
k	Stem segment
LAD	Left anterior descending artery
L_i	Segment length
m_i	Microspheres mapped to a segment
M_k	Total number of microspheres that passed through a stem segment
N^k	Total number of downstream segments for a stem segment
p	Factor relating number of microspheres to the measured flow rate during microsphere injection
Q	Hyperemic flow
Q_{200}	Reference flow
Q_k	Flow through a stem segment
Q_r	Flow at a truncation level
Q_s	Flow through a stenosed vessel
r	Truncation level
r_i	Segment radius
V	Cumulative volume of the distal arterial tree
v_i	Segmental volume
V_k	Crown volume for stem segment k

MATERIALS AND METHODS

Canine coronary datasets. Five healthy canine hearts were obtained from a series of physiological experiments carried out according to a protocol that was approved by the Institutional Animal Care and Use Committee of the University of Utrecht Medical Center. Details on experimental procedures and animal handling are described elsewhere (22, 23). After premedication (medetomidine 0.03 mg/kg im, ketamine 0.03 mg/kg im, and atropine 0.5 mg im), the animals were anesthetized (sufentanil 10 $\mu g \cdot kg^{-1} \cdot h^{-1}$ iv), intubated, and mechanically ventilated with supplemental oxygen. Anesthesia was maintained by using a mixture of propofol (24 $mg \cdot kg^{-1} \cdot h^{-1}$ iv) and sufentanil (3 $\mu g \cdot kg^{-1} \cdot h^{-1}$ iv). No muscle relaxants were used. The heart was exposed by left thoracotomy via the fourth intercostal space. At the conclusion of the experimental protocol, ~100,000 carmine fluorescent microspheres (15-μm diameter, 582-nm excitation/614-nm emission wavelength, Invitrogen Life Technologies) were infused into the left anterior descending artery (LAD) during adenosine-induced maximal hyperemia, while volumetric flow proximal to the injection site was measured (Transonic Systems). Hereafter, heparin was administered, and the animal was killed by vena cava puncture. Cardiac contraction was stopped in diastolic arrest by inducing ventricular fibrillation using a 9-V battery. The heart was excised and the right and left main coronary arteries were cannulated and perfused with a buffered solution containing adenosine for vasodilation of the microcirculation, until the efflux was clear from blood. The coronary arteries were filled at physiological pressure (80–100 mmHg) with a fluorescent (Potomac Yellow, 440 nm excitation/490 nm emission, Radiant Colour) cast material (Batson no. 17, Polysciences) consisting of a monomer base solution, a catalyst, and a promoter as described previously (14). The cast material was allowed to harden over a period of 24 h at ambient temperature. The heart was embedded in 5% carboxymethylcellulose sodium solvent (Brunschwig Chemie) mixed with 5% Indian ink (Royal Talens) and frozen at −20°C for cryomicrotome processing.

The imaging cryomicrotome. The cryomicrotome setup and episcopic imaging procedure were described in detail by Spaan et al. (14). Some modifications were implemented since then and used in the present study (20). In brief, the frozen heart was mounted with its long axis perpendicular to the cutting plane and cut, from base to apex, at 25-μm slice thickness using a motorized automated cutting mechanism. After each cut, the block face of the remaining bulk material was illuminated with two clusters of 7 power light-emitting diodes (Luxeon V, Star, Royal Blue, Lumileds Lighting) with a central wavelength of 440 nm (cast) and 560 nm (microspheres) and imaged with a pixel size of 25 μm using a 4,096 × 4,096 pixel CCD camera (Apogee Alta U-16) equipped with a variable-focus lens (Nikon 70–180 mm). After each cut, a black and white photo of the heart as well as emission images of the fluorescent cast material and microspheres were acquired after filtering the emission light at 505 nm and 635 nm, respectively. Sequential images were combined to yield a registered image stack representing the detailed 3D virtual morphology of the coronary vascular network, microsphere locations, and surrounding tissue.

Image restoration. Fluorescence images are degraded due to scattering of emission light in the tissue, lens blurring, and light emanating from structures beneath the imaged surface. For the arterial cast images, image restoration entailed deconvolution with a system-specific point spread function (12). Correction of the image stack was performed in the spatial domain using a 3D iterative deconvolution program written in CUDA (NVidia) (3). As this deconvolution would reduce microspheres to single pixels, making them indistinguishable from background noise, the microsphere images were processed by a slicewise removal of the transparency artifacts followed by microsphere detection using a dedicated algorithm (21).

Vascular tree segmentation and quantification. After deconvolution, the vessel outlines were skeletonized using a topology-preserving thinning algorithm (10). The resulting centerlines were automatically checked and corrected for overconnected branch points and spurious branches (24). Points on the centerlines were classified according to their nearest-neighbor connections, as end points, with one neighbor; midpoints, with two neighbors; and bifurcations, in case of three neighbors. Higher orders of connectivity due to thinning artifacts were replaced by bifurcations. Vessel segments were defined between consecutive non-midpoints. Tree segmentation was visually checked by overlaying the segmented tree and the 3D images of the vascular cast in 3D. The segmented tree represented the 3D topological vascular network (22).

Local diameters were determined by examining the cross-sectional intensity profile along 64 radial vectors perpendicular to the segment centerline for each midpoint. The full width at half-maximum intensity along each vector was found and averaged to yield the midpoint diameter. The cross-sectional area of the segment was assumed to be

Downloaded from http://ajpheart.physiology.org/ by 10.220.33.2 on January 3, 2017

circular with a constant segmental diameter defined by averaging over its midpoint diameters.

Q-V scaling law determination. The coronary arterial system was reconstructed in 3D down to the smallest observable segment with a radius of 25 μm. As illustrated in Fig. 1, each detected microsphere was then mapped to the nearest segment centerline to determine the relative perfusion of each segment.

In order to ensure a uniform terminal segment radius, the smallest vessels were limited to a radius of 50 μm. The volume of each individual segment (v_i) was determined from its average radius (r_i) and length (L_i) assuming a cylindrical shape. For a chosen stem segment k, all N^k downstream segments were identified and their volumes summed to yield the corresponding crown volume (V_k). Hence the total vascular crown volume V_k distal to a stem segment is given by

$$V_k = \sum_{i=1}^{N^k} v_i \quad (1)$$

The total number of microspheres (M_k) that passed through stem segment k was determined from the sum of all microspheres mapped to the corresponding crown segments, m_i, as

$$M_k = \sum_{i=1}^{N^k} m_i \quad (2)$$

Segmental flow Q_k was assessed from the number of microspheres that passed through a segment according to

$$Q_k = pM_k \quad (3)$$

with the factor p relating number of microspheres to the measured flow rate during microsphere injection.

The scaling law between flow and cumulative vascular volume was obtained by fitting the corresponding Q_k and V_k data with the exponential relation

$$Q_k = \alpha V_k^{\beta} \quad (4)$$

to obtain the value of scaling factor α and exponent β.

Simulating the effect of limited image resolution by vessel truncation. The typical terminal vessel radius evaluated from coronary angiograms in a previous study was 250 μm and larger (7), whereas the resolution of computed tomography angiography is in the order of 600 μm (5). We simulated limited image resolution by excluding vasculature below a threshold radius from the volume determination, as illustrated in Fig. 2. For stem segments of 1,000 μm radius and larger, the truncation radius of terminal segments was increased from 50 to 100 μm and then in steps of 100 μm up to a maximum of 1,000 μm. The resulting crown volume obtained with threshold radius r is referred to as V_r. Scaling factor α and exponent β (*Eq. 4*) were then determined from these truncated vascular tree models as a function of truncation radius and, hence, simulated limits in image resolution.

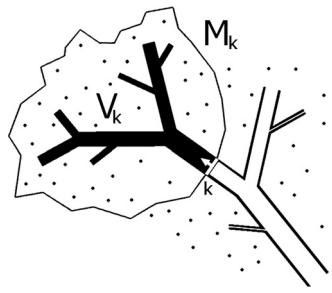

Fig. 1. Schematic representation of a subtree with stem segment k and its corresponding distal crown volume, V_k (black vessels). Microspheres within the crown contour are mapped to the distal vascular tree according to the distance to the nearest vessel centerline as a relative measure of perfusion, M_k, through the stem segment.

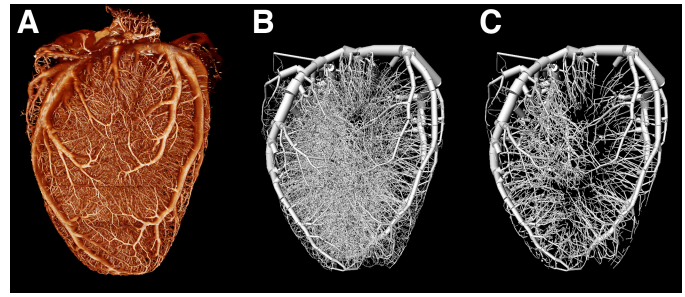

Fig. 2. *A*: raw vascular cast data obtained by cryomicrotome imaging of the full coronary tree. *B*: segmented representation of the raw data down to 50-μm-radius vessels. *C*: representation of the dataset truncated at 200-μm vessel radius.

Since the crown volume of subtrees increases with the size of the feeding stem segment, the effect of terminal segment truncation was also explored in the LAD network of one heart for crown volumes distal to all stem segments larger than 200-μm radius.

Truncation-induced error in prediction of maximal flow and FFR. In order to quantify the effect of resolution-dependent scaling parameters on hyperemic flow prediction, we determined the relative error when estimating flow for values of α and β resulting from a truncation radius r compared with using 200-μm radius truncation with fixed scaling law coefficients (α_{200} and β_{200}) as a reference. This value was chosen as typical terminal vessel radius that can be quantified from clinical imaging modalities. The relative systematic error can be written as:

$$Q_{error}(\%) = \left[\frac{\alpha_{200} V^{\beta 200}}{\alpha_r V^{\beta_r}} - 1\right] 100 \quad (5)$$

The error estimate was investigated for physiological crown volumes ranging from 0 to 1 ml (22).

We also analyzed the effect of truncation-induced errors in estimated maximal flow on FFR. Using the reference flow assessed at radius truncation of 200 μm (Q_{200}) and Q_s as hyperemic flow through a stenosed artery, a reference FFR was defined as

$$FFR_{ref} = \frac{Q_s}{Q_{200}} = 0.8 \quad (6)$$

FFR_{ref} was assigned a value of 0.8, representing the threshold value for clinical decision making (25).

When estimated at truncation level r, FFR becomes

$$FFR = \frac{Q_s}{Q_r} \quad (7)$$

By substituting *Eq. 6* into *Eq. 7*, the FFR prediction compared with the reference value FFR = 0.8 can then be expressed as

$$FFR = 0.8 \times \frac{Q_{200}}{Q_r} \quad (8)$$

Statistical methods. The power law factor α and exponent β were obtained from linear regression of log-transformed microsphere flow data and crown volumes, using data for multiple stem segments in each heart and after pooling data over the five hearts. The Spearman correlation coefficient was determined from linear regression analysis. A nonparametric one-way repeated-measures analysis of variance followed by post hoc analysis using Dunn's test was used to assess changes in α and β. A value of $P < 0.05$ was considered statistically significant. All statistical analyses were performed in Graphpad Prism (GraphPad Software, La Jolla, CA).

Downloaded from http://ajpheart.physiology.org/ by 10.220.33.2 on January 3, 2017

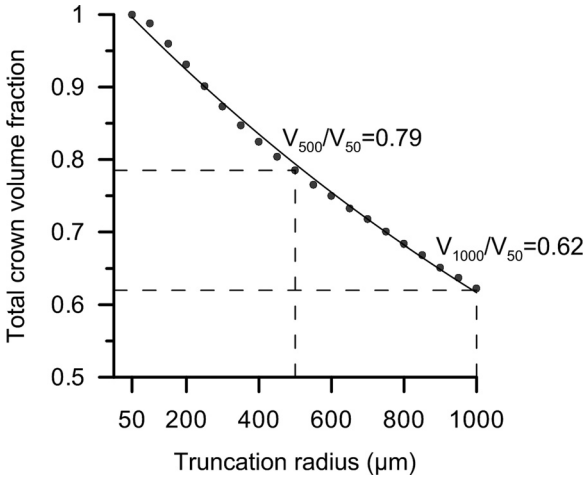

Fig. 3. Relationship between total vascular volume fraction and truncation radius for all hearts. There is a mild exponential increase in total crown volume fraction toward smaller truncation radii. The volume at 500-μm truncation radius (V_{500}) was on average 79% of the crown volume assessed at 50-μm truncation (V_{50}) and only 62% at 1,000-μm truncation (V_{1000}).

RESULTS

Impact of terminal segment truncation on total coronary crown volume. Inclusion of smaller vessel segments (higher imaging resolution) was expected to yield larger coronary arterial volumes. Figure 3 quantifies this relation, showing that relative to the coronary volume truncated at vessels of 50-μm radius, only 62% of the total arterial volume was located in vessels larger than 1,000 μm in radius and 79% in vessels larger than 500 μm in radius.

Impact of radius truncation on stem-dependent crown volume. Figure 4*A* shows the relation between crown volume and corresponding stem radius for an LAD arterial network truncated at 50 μm and 500-μm terminal segment radius. The difference between the two crown volumes increases with decreasing stem radius. The relation between the two truncated crown volumes is depicted in Fig. 4*B*, where each point represents data from a different stem. V_{500} crown volumes were progressively smaller than V_{50} volumes.

Relationship between flow and crown volume. The truncated crown volumes (V_{50}, V_{500}, and V_{1000}) for all stem segments and their corresponding hyperemic flows are plotted in Fig. 5 for a typical example of an LAD coronary tree, containing 100 of such segments. Fit of the allometric relation (*Eq. 4*) to this tree resulted in a scaling factor α of 56.23, 63.09, and 57.54 and an exponent β of 0.79, 0.71, and 0.55 for these three truncation radii, respectively. Consequently, the log-log Q-V relation became steeper for smaller truncation levels.

Evaluation of the Q-V scaling law for all hearts and truncation levels revealed a large intersubject variability in scaling factor α with increasing truncation radius, without a significant change in the median value (Fig. 6*A*). In contrast, a nonlinear decline in exponent β was observed with increasing truncation radius (Fig. 6*B*). The value of β was significantly lower for truncation radii above 500 μm compared with its value derived at 50-μm truncation ($P < 0.05$).

Error estimate of flow and FFR related to truncation level. Larger errors in flow estimates and FFR prediction occur for greater mismatch with the reference β adapted to the image resolution. For truncation levels less than an assumed 200-μm reference level (larger values of β) the hyperemic flow was overestimated, and for larger truncation levels (smaller values of β) stem flow was underestimated, as depicted in Fig. 7*A*. These errors increased for smaller crown volumes. The corresponding FFR prediction as defined by *Eq. 8* is depicted in Fig. 7*B* with a reference FFR of 0.8 assigned for a reference stem flow for truncation at 200 μm. FFR was underestimated for larger and overestimated for smaller truncation radii, again with larger deviations at smaller crown volumes.

DISCUSSION

This study confirms the allometric relation between diameter of the feeding coronary stem segment and its crown volume, i.e., the total volume of the distal tree as visible during imaging. Moreover, we observed a similar allometric relation between crown volume and stem flow. Especially the second relationship is relevant, since it is used in applications for noninvasive determination of hyperemic flow and FFR. We demonstrated that the exponent in this latter relation depends on the truncation level of the downstream tree. This implies that this exponent should be adapted to the resolution of the imaging modality used to assess crown volume when predicting hyperemic flow or FFR.

Impact of image resolution on scaling law. The allometric hyperemic flow-volume relation is formulated as $Q = \alpha V^{\beta}$,

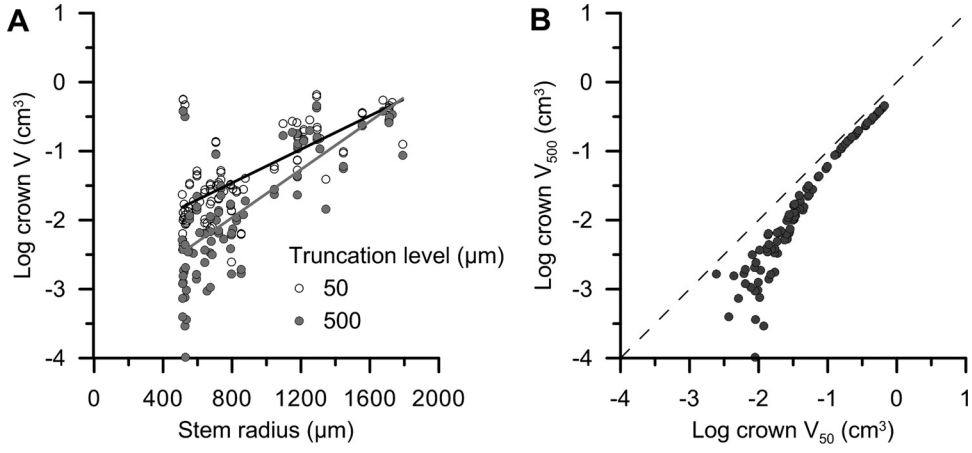

Fig. 4. *A*: crown volume increases with larger stem segment radius. The difference between volumes assessed at truncation levels 50 μm (white dots) and 500 μm (gray dots) is larger with decreasing stem radius. Linear fits were $Y = 0.001 \times X - 2.43$ ($r = 0.73$) for 50 μm (black) and $Y = 0.002 \times X - 3.36$ ($r = 0.75$) for 500 μm (gray) truncation. *B*: comparison of crown volumes belonging to the same stem, truncated at terminal vessel radius of 50 (V_{50}) and 500 μm (V_{500}), respectively. The relationship between the crown volumes is increasingly affected at smaller crown volumes; the data points deviate from the identity (dashed line). Data are from the LAD of one heart for stem segments larger than 1,000 μm.

Downloaded from http://ajpheart.physiology.org/ by 10.220.33.2 on January 3, 2017

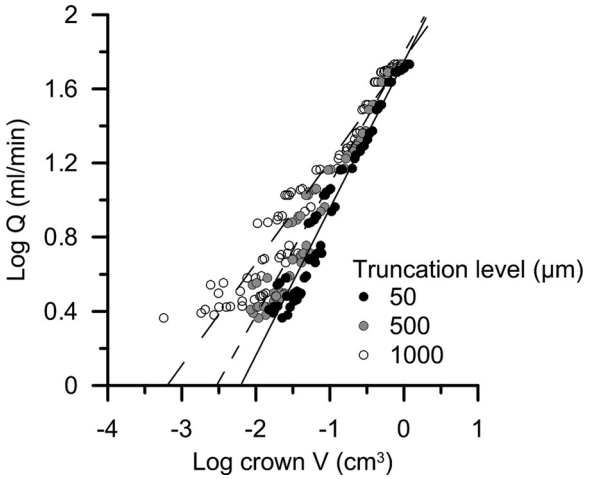

Fig. 5. Hyperemic flow (Q) vs. crown volume (V) for three different truncation radii in the LAD of one heart. The relationship becomes less steep with increasing vessel radius truncation. Respective log-log fits for 50-, 500-, and 1,000-μm truncation were $Q = 0.79 \cdot V + 1.75$ ($r = 0.98$), $Q = 0.71 \cdot V + 1.80$ ($r = 0.98$), and $Q = 0.55 \cdot V + 1.76$ ($r = 0.97$). This resulted in a scaling factor α of 56.23, 63.09, and 57.54 and an exponent β of 0.79, 0.71, and 0.55 for these respective truncation radii.

including scaling factor α and exponent β. Although different between hearts, α was independent of vessel truncation. In contrast, the exponent β in our study decreased from 0.79 to 0.55 for truncation radii ranging from 50 to 1,000 μm. A value of 3/4 (0.75) for the exponent was previously suggested based on the measured relationship between flow and segment length and the derived relationship between segment length and cumulative arterial volume (31). This value was validated by angiographic imaging at the limited resolution of 500 μm (7, 15, 30). Using theoretical derivation based on rules for branching at bifurcations, a value of 7/9 (0.78) has been suggested (4), which agrees well with $\beta = 0.79$ found at our smallest truncation radius (50 μm).

The impact of limited spatial resolution, by truncating vessels with small diameters, was previously investigated for allometric scaling laws between regional myocardial mass and arterial lumen volume or cumulative arterial branch length, i.e., between strictly morphological data (6). This analysis showed no significant effect of truncation between 600 and 1,400 μm on the exponent. The effect of vessel truncation on the Q-V scaling law was only indirectly investigated in that study. Flow simulations on a computer model of an entire porcine coronary arterial tree down to the capillary level resulted in predicted values of β in the range of 0.7–0.77 when the smallest diameters included in the model were varied between 8 and 500 μm (8). This agrees well with the corresponding range of our β values obtained from actual coronary trees and measured stem flow.

Application of allometric scaling laws to predict functional stenosis severity. The feasibility of predicting FFR using angiographic image data, where hyperemic flow is estimated from the crown volume based on a scaling law, has been evaluated in animal experiments (26). Initially, regional hyperemic flow in diseased coronary arteries was assessed by first-pass analysis of angiographic contrast and densitometric volume measurements of the arterial tree (9). The region of interest was selected in the angiographic images by following the outlines of visible epicardial arteries down to an arterial diameter of ~0.5 mm (7). This method was extended to predict FFR from angiographic data (26, 28), using hyperemic flow predictions for the theoretically undiseased vessel based on scaling laws. Our findings highlight the importance of image resolution, since the exponent of the Q-V scaling law depends on the smallest diameter contained in the volume determination. Crown volumes and hence hyperemic flow are likely underestimated if an exponent for a higher image resolution is used in the volume estimation. It is important to note that we applied selective vessel truncation to a high-resolution "ideal" data set. Our findings of changes in the exponent of the hyperemic flow-crown volume scaling law refer to the smallest segmented vessel size after truncation.

In medical imaging, the smallest segmented vessels are usually much larger than the spatial resolution of the imaging technique. Resolving small vessels is further limited by imaging artifacts such as vessel motion or partial volume effects, especially in CT imaging with a lower inherent resolution. Depending on segmentation algorithms, such artifacts can result in an over- or underestimation of the vascular size and volume. In practical applications, the exponent of the scaling law should hence be adapted to the smallest vessel size included in the analysis.

In the present study, the allometric scaling law relating hyperemic flow to arterial crown volume (7) was used to assess

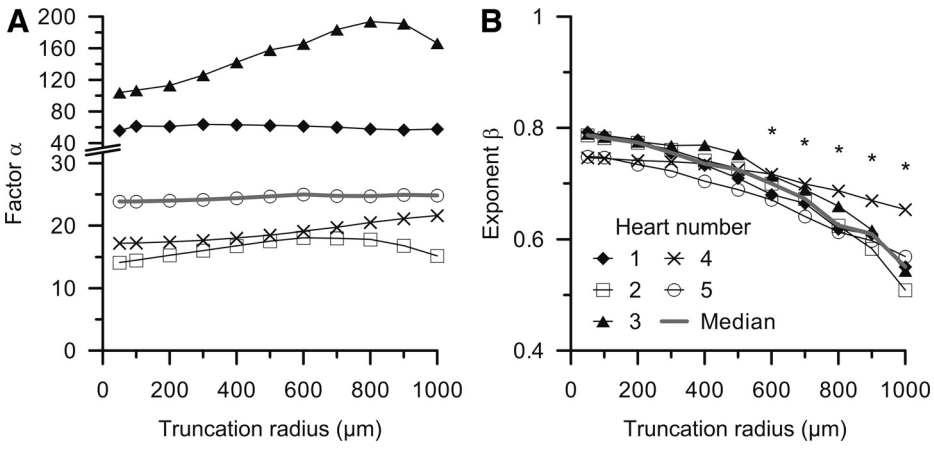

Fig. 6. *A*: scaling factor α as a function of truncation radius obtained for stem segments with a radius greater than 1,000 μm. The median of factor α remained unchanged for increased radius truncation. *B*: exponent β as a function of truncation radius. A significant decline of the median value was observed with larger truncation radii. *$P < 0.05$ vs. 50-μm truncation radius.

Downloaded from http://ajpheart.physiology.org/ by 10.220.33.2 on January 3, 2017

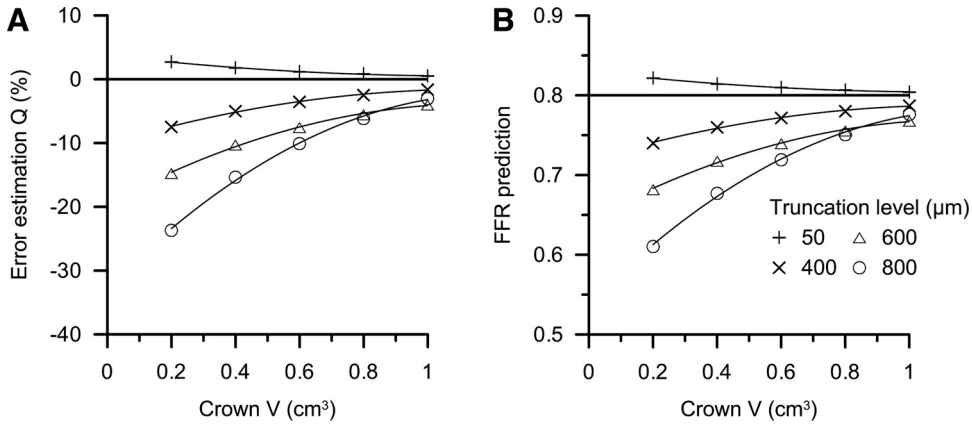

Fig. 7. *A*: effect of vessel truncation on deviations in flow (Q) prediction for different crown volumes, relative to hyperemic flow assessed at 200-μm truncation radius (horizontal line). *B*: FFR prediction for hyperemic flow assessed at different levels of radius truncation. Reference FFR = 0.8 (horizontal line) was assigned for hyperemic flow derived at 200-μm truncation level. With decreasing crown volumes, stem flow and FFR predictions progressively deviate from reference values derived at 200-μm truncation radius.

possible consequences of limited vessel resolution on hyperemic flow and FFR estimation.

In contrast, recent studies for noninvasive FFR computation from coronary CT angiography (16) are based on total rest coronary flow relative to left ventricular mass extracted from CT images (1). An allometric relation between stem diameter and baseline flow is employed to distribute relative basal outlet coronary resistances over the segmented branches. Hyperemic flow is then estimated assuming a predictable microcirculatory response to adenosine, whereas individual patients show a large spread around the group average (5, 17).

We cannot verify these relationships on the basis of our data, since we have not determined myocardial mass or baseline flow. However, it is conceivable that our findings extend to other scaling laws that are based on segmentation of coronary vascular structures down to the limits imposed by the resolution of the imaging modality.

Influence of coronary branching heterogeneity and physiological conditions. The subendocardial layer of the heart contains a larger vascular volume compared with the midmyocardial and subepicardial layers (29). This raises the question whether transmural differences in crown volume influence the scaling law exponent as well. We addressed this question by deriving the log-log relation between crown volumes with truncation radii of 50 and 200 μm, respectively, for subendocardial and subepicardial subtrees (Fig. 8). For stems of transmural penetrating arteries, perfused layers were assigned by their myocardial penetration depth (23). Subendocardial trees penetrated transmurally to the endocardium, and subepicardial trees reached no further than one-third into the myocardium. Although the results are only from a single heart, a clear differential effect of truncation in these two layers can be observed, with a more pronounced effect on subepicardial branches. This difference is probably related to the higher vascular density at the subendocardium (23). Therefore, the choice of β for regional flow estimation may also have to include the transmural location of the vascular tree. We could not establish reliable Q-V relations for these two regions because the microsphere density was not sufficient.

Hyperemic coronary flow depends on not only tree morphology, but also cardiac function. Vascular conductance varies with diastolic time fraction and decreases with increasing heart rate and decreasing coronary pressure, particularly at the subendocardium (2). A detailed discussion of these aspects can be found in recent reviews (13, 19). It remains to be established to what extent this affects flow estimation by allometry applied to coronary image data obtained in specific patient groups or conditions.

Study limitations. Vascular casting may suffer from incomplete filling of the vascular tree due to air bubbles in the cast material and possible residual blood clots in the vasculature. Distributions of terminal segment radii were used to investigate the quality of overall filling. The datasets presented in this study were selected from a larger group of animals based on the quality of filling.

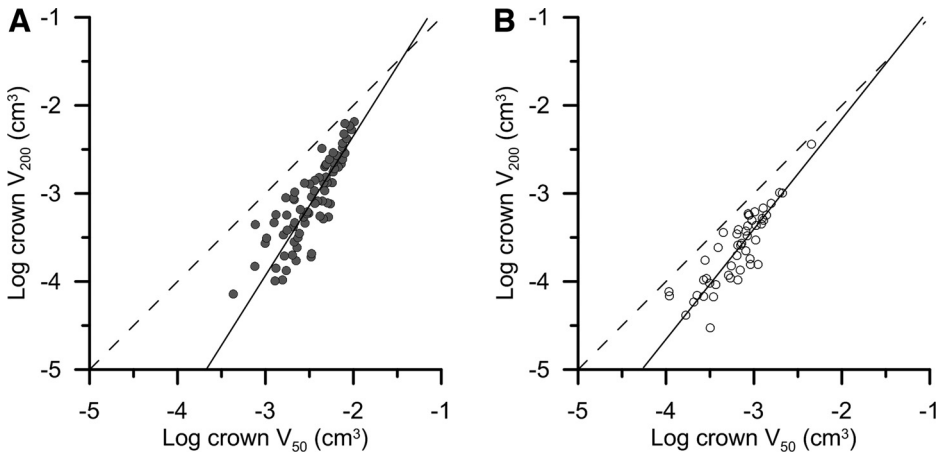

Fig. 8. Relation between crown volume for 50-μm and 200-μm radius truncation for subendocardial (*A*) and subepicardial branches (*B*). Vessel truncation has a stronger effect on the endocardial subtrees due to the higher vascular density. Linear fits were $Y = 1.59 \times X + 0.83$ ($r = 0.83$) for endocardial and $Y = 1.25 \times X + 0.35$ ($r = 0.88$) for epicardial branches.

Downloaded from http://ajpheart.physiology.org/ by 10.220.33.2 on January 3, 2017

A small underestimation in the length of curved segments may have occurred, since arterial length was determined as the Euclidian distance between segmental start and end point. However, for equal curvature in large and small vessels, this would only affect α and not β.

The data presented were obtained from the vasculature in the LAD flow territory of canine hearts. Yet, Molloi and Wong (8) reported comparable Q-V relations for the right and left coronary artery trees.

In conclusion, a correct allometric relation is required for proper estimation of hyperemic blood flow and FFR from tree morphology. Analysis of detailed 3D vascular structures and microsphere flow obtained from high-resolution cryomicrotome images allowed investigation of these allometric scaling laws. The Q-V scaling law exponent β was shown to decrease when truncating at larger vessel diameters during volume determination. Therefore, the scaling law exponent β should be adapted to image resolution.

ACKNOWLEDGMENTS

Present address of P. van Horssen: Department of Physics and Medical Technology, VU University Medical Center, Amsterdam, The Netherlands.

Present address of J. P. H. M. van den Wijngaard: Central Clinical Chemistry Laboratory, Leiden University Medical Center, Leiden, The Netherlands.

GRANTS

This work was supported by grants from the Center for Translational Molecular Medicine (CTMM), project EMINENCE (Grant 01C-204), the European Commission (FP7-ICT-2007/2013 no. 224495: euHeart), the Netherlands Organization for Health Research and Development (ZonMw 91105008 and 91112030), and the Netherlands Heart Foundation (NHS 2006B226). J. P. H. M. van den Wijngaard was funded by a Veni grant from the Netherlands Organization for Scientific Research (NWO/ZonMw 91611171).

DISCLOSURES

No conflicts of interest, financial or otherwise, are declared by the author(s).

AUTHOR CONTRIBUTIONS

Author contributions: P.v.H., J.P.v.d.W., I.E.H., J.A.S., and M.S. performed experiments; P.v.H., M.G.v.L., and M.S. analyzed data; P.v.H., M.G.v.L., J.P.v.d.W., E.V., J.A.S., and M.S. interpreted results of experiments; P.v.H., M.G.v.L., and M.S. prepared figures; P.v.H., M.G.v.L., and M.S. drafted manuscript; P.v.H., M.G.v.L., J.P.v.d.W., E.V., J.A.S., and M.S. edited and revised manuscript; P.v.H., M.G.v.L., J.P.v.d.W., E.V., J.A.S., and M.S. approved final version of manuscript; J.A.S. and M.S. conception and design of research.

REFERENCES

1. **Choy JS, Kassab GS.** Scaling of myocardial mass to flow and morphometry of coronary arteries. *J Appl Physiol (1985)* 104: 1281–1286, 2008.
2. **Fokkema DS, VanTeeffelen JW, Dekker S, Vergroesen I, Reitsma JB, Spaan JA.** Diastolic time fraction as a determinant of subendocardial perfusion. *Am J Physiol Heart Circ Physiol* 288: H2450–H2456, 2005.
3. **Geenen T, van Horssen P, Spaan JAE, Siebes M, van den Wijngaard JPHM.** Iterative deblurring of large 3D datasets from cryomicrotome imaging using an array of GPUs. In: *GPU Solutions to Multi-scale Problems in Science and Engineering*, edited by Yuen DA, Wang L, Chi X, Johnsson L, Ge W, Shi Y. Berlin: Springer, 2013, p. 573–585.
4. **Huo Y, Kassab GS.** Intraspecific scaling laws of vascular trees. *J R Soc Interface* 9: 190–200, 2012.
5. **Johnson NP, Kirkeeide RL, Gould KL.** Coronary anatomy to predict physiology fundamental limits. *Circ Cardiovasc Imag* 6: 817–832, 2013.
6. **Le H, Wong JT, Molloi S.** Estimation of regional myocardial mass at risk based on distal arterial lumen volume and length using 3D micro-CT images. *Comput Med Imag Graph* 32: 488–501, 2008.
7. **Molloi S, Chalyan D, Le H, Wong JT.** Estimation of coronary artery hyperemic blood flow based on arterial lumen volume using angiographic images. *Int J Cardiovasc Imaging* 28: 1–11, 2012.
8. **Molloi S, Wong JT.** Regional blood flow analysis and its relationship with arterial branch lengths and lumen volume in the coronary arterial tree. *Phys Med Biol* 52: 1495–1503, 2007.
9. **Molloi S, Zhou Y, Kassab GS.** Regional volumetric coronary blood flow measurement by digital angiography: in vivo validation. *Acad Radiol* 11: 757–766, 2004.
10. **Palagyi K, Kuba A.** A 3D 6-subiteration thinning algorithm for extracting medial lines. *Pattern Recogn Lett* 19: 613–627, 1998.
11. **Pijls NH, De Bruyne B, Peels K, Van Der Voort PH, Bonnier HJ, Bartunek JKJJ, Koolen JJ.** Measurement of fractional flow reserve to assess the functional severity of coronary-artery stenoses. *N Engl J Med* 334: 1703–1708, 1996.
12. **Rolf MP, ter Wee R, van Leeuwen TG, Spaan JA, Streekstra GJ.** Diameter measurement from images of fluorescent cylinders embedded in tissue. *Med Biol Eng Comput* 46: 589–596, 2008.
13. **Spaan JA, Piek JJ, Hoffman JI, Siebes M.** Physiological basis of clinically used coronary hemodynamic indices. *Circulation* 113: 446–455, 2006.
14. **Spaan JA, ter Wee R, van Teeffelen JW, Streekstra G, Siebes M, Kolyva C, Vink H, Fokkema DS, VanBavel E.** Visualisation of intramural coronary vasculature by an imaging cryomicrotome suggests compartmentalisation of myocardial perfusion areas. *Med Biol Eng Comput* 43: 431–435, 2005.
15. **Takarada S, Zhang Z, Molloi S.** An angiographic technique for coronary fractional flow reserve measurement: in vivo validation. *Int J Cardiovasc Imaging* 29: 535–544, 2013.
16. **Taylor CA, Fonte TA, Min JK.** Computational fluid dynamics applied to cardiac computed tomography for noninvasive quantification of fractional flow reserve: scientific basis. *J Am Coll Cardiol* 61: 2233–2241, 2013.
17. **Tu S, Barbato E, Koszegi Z, Yang J, Sun Z, Holm NR, Tar B, Li Y, Rusinaru D, Wijns W, Reiber JH.** Fractional flow reserve calculation from 3-dimensional quantitative coronary angiography and TIMI frame count: a fast computer model to quantify the functional significance of moderately obstructed coronary arteries. *JACC Cardiovasc Interv* 7: 768–777, 2014.
18. **Tu S, Bourantas CV, Norgaard BL, Kassab GS, Koo BK, Reiber JH.** Image-based assessment of fractional flow reserve. *EuroIntervention* 11, *Suppl V: V50–V54, 2015*.
19. **van de Hoef TP, Meuwissen M, Escaned J, Davies JE, Siebes M, Spaan JA, Piek JJ.** Fractional flow reserve as a surrogate for inducible myocardial ischaemia. *Nat Rev Cardiol* 10: 439–452, 2013.
20. **van den Wijngaard JP, Schwarz JC, van Horssen P, van Lier MG, Dobbe JG, Spaan JA, Siebes M.** 3D Imaging of vascular networks for biophysical modeling of perfusion distribution within the heart. *J Biomech* 46: 229–239, 2013.
21. **van Horssen P, Siebes M, Hoefer I, Spaan JA, van den Wijngaard JP.** Improved detection of fluorescently labeled microspheres and vessel architecture with an imaging cryomicrotome. *Med Biol Eng Comput* 48: 735–744, 2010.
22. **van Horssen P, Siebes M, Spaan JA, Hoefer IE, van den Wijngaard JP.** Innate collateral segments are predominantly present in the subendocardium without preferential connectivity within the left ventricular wall. *J Physiol* 592: 1047–1060, 2014.
23. **van Horssen P, van den Wijngaard JP, Brandt MJ, Hoefer IE, Spaan JA, Siebes M.** Perfusion territories subtended by penetrating coronary arteries increase in size and decrease in number toward the subendocardium. *Am J Physiol Heart Circ Physiol* 306: H496–H504, 2014.
24. **van Horssen P, van den Wijngaard JPHM, Nolte F, Hoefer I, Haverslag R, Spaan JAE, Siebes M.** Extraction of coronary vascular tree and myocardial perfusion data from stacks of cryomicrotome images. In: *Functional Imaging and Modeling of the Heart*, edited by Ayache N, Delingette H, Sermesant M. Berlin: Springer, 2009, p. 486–494.
25. **Windecker S, Kolh P, Alfonso F, Collet JP, Cremer J, Falk V, Filippatos G, Hamm C, Head SJ, Juni P, Kappetein AP, Kastrati A, Knuuti J, Landmesser U, Laufer G, Neumann FJ, Richter DJ, Schauerte P, Sousa Uva M, Stefanini GG, Taggart DP, Torracca L, Valgimigli M, Wijns W, Witkowski A.** 2014 ESC/EACTS Guidelines on myocardial revascularization: The Task Force on Myocardial Revascularization of the European Society of Cardiology (ESC) and the European Association for Cardio-Thoracic Surgery (EACTS), developed with the

Downloaded from http://ajpheart.physiology.org/ by 10.220.33.2 on January 3, 2017

special contribution of the European Association of Percutaneous Cardiovascular Interventions (EAPCI). *Eur Heart J* 35: 2541–2619, 2014.
26. **Wong J, Le H, Suh W, Chalyan D, Mehraien T, Kern M, Kassab G, Molloi S.** Quantification of fractional flow reserve based on angiographic image data. *Int J Cardiovasc Imaging* 28: 13–22, 2012.
27. **Wong JT, Ducote JL, Xu T, Hassanein MT, Molloi S.** Automated technique for angiographic determination of coronary blood flow and lumen volume. *Acad Radiol* 13: 186–194, 2006.
28. **Wong JT, Molloi S.** Determination of fractional flow reserve (FFR) based on scaling laws: a simulation study. *Phys Med Biol* 53: 3995, 2008.
29. **Wusten B, Buss DD, Deist H, Schaper W.** Dilatory capacity of the coronary circulation and its correlation to the arterial vasculature in the canine left ventricle. *Basic Res Cardiol* 72: 636–650, 1977.
30. **Zhang Z, Takarada S, Molloi S.** Quantification of absolute coronary flow reserve and relative fractional flow reserve in a swine animal model using angiographic image data. *Am J Physiol Heart Circ Physiol* 303: H401–H410, 2012.
31. **Zhou Y, Kassab GS, Molloi S.** On the design of the coronary arterial tree: a generalization of Murray's law. *Phys Med Biol* 44: 2929–2945, 1999.

Downloaded from http://ajpheart.physiology.org/ by 10.220.33.2 on January 3, 2017